IEEE Access
Multidisciplinary | Rapid Review | Open Access Journal

Received May 26, 2021, accepted June 21, 2021, date of publication June 29, 2021, date of current version July 8, 2021.

Digital Object Identifier 10.1109/ACCESS.2021.3093460

5G K-SimSys for Open/Modular/Flexible System-Level Simulation: Overview and Its Application to Evaluation of 5G Massive MIMO

JAEWON LEE[1], MINSIG HAN[1], MINJOONG RIM[2], AND CHUNG G. KANG[1], (Senior Member, IEEE)

[1]School of Electrical Engineering, Korea University, Seoul 02841, Republic of Korea
[2]Information and Communication Engineering, Dongguk University, Seoul 04620, Republic of Korea

Corresponding author: Chung G. Kang (ccgkang@korea.ac.kr)

This work was supported in part by 'the Cross-Ministry Giga KOREA Project' grant funded by the Korea government (Ministry of Science and ICT) (No. GK18S0400, Research and Development of Open 5G Reference Model) and in part by the Brain Korea 21 Plus Project in 2020.

ABSTRACT 5G K-SimSys is a system-level simulator which has been designed and implemented to provide an open platform and a tractable testbed for evaluating the system-level performance of 5G standard. In this paper, we present its design overview with the overall modular structure, including the functionality of the flexible modules. Meanwhile, massive multi-input multi-output (MIMO) is a key technology for improving the spectral efficiency of 5G systems. While massive MIMO has been standardized in 3GPP Rel-13 (LTE-Advanced Pro), the next generation of massive MIMO standard is now available in Rel-16, a.k.a New Radio (NR) interface, with further improvement by introducing more antenna elements over the higher frequency band. In particular, the beam-based air interface for above 6 GHz band involves various antenna configurations and feedback schemes, requiring a more complex testbed for system-level performance evaluation. This paper examines the multi-antenna technologies in 3GPP NR specification to develop its system-level model in 5G K-SimSys in order to test the factors affecting performance in the corresponding environments through various embodiments. In the simulation results, the baseline performance for massive MIMO in NR is evaluated by changing the number of antenna ports and the number of spatial multiplexing layers in different experimental environments. Particularly, the effect of vertical beamforming on interference is evaluated for Full Dimension MIMO (FD-MIMO). In order to demonstrate that 5G K-SimSys is an easy-to-design simulator that facilitates modification and reconfiguration, owing to its modularized and customized structure, we consider the proposed bandwise analog beamforming (BAB) scheme. The modular and flexible structure immediately allows implementation of virtual modules for bandwise analog beamforming by reusing the elementary modules as hierarchically designed simulator objects.

INDEX TERMS 3GPP, 5G, K-SimSys, beamforming, massive MIMO, new radio, system-level simulation.

I. INTRODUCTION

Performance evaluation of a cellular system involves simulations at different levels, e.g., link-level simulation (LLS) for block error rate (BLER) and system-level simulation (SLS) for average system throughput, under various environments modeled by channel measurements [1]–[5]. Of these, LLS focuses only on the physical (PHY) layer of the communication system. Therefore, simulations such as channel coding, MIMO processing, multicarrier modulation, channel estimation, and equalization are performed using fixed-point point-to-point channels [6], e.g., cluster delay line and tapped delay line channel models, without dealing with any high-level resource allocation for packet scheduling among the multiple user equipments (UEs). LLS could also be implemented for multi-point communication evaluation; however, its computational complexity becomes prohibitively high as the considered number of points increases.

The associate editor coordinating the review of this manuscript and approving it for publication was Li Zhang.

In contrast, SLS evaluates the system-level performance for the complex multi-user communication scenarios, on both PHY and medium access control (MAC) layers. PHY layer performance is abstracted by link-to-system mapping for reducing its computational complexity, which allows prediction of BLER performance based upon the received signal-to-noise and interference ratio (SINR) in any channel condition. Thus, LLS and SLS play a complementary role in calculating the SINR for the system-level performance, as specified by simulation methodology for evaluation of IMT-2020 specification in the International Telecommunication Union [7].

5G mobile communication systems consider three service scenarios, including eMBB, mMTC, and URLLC with eight key performance indicators (KPIs), besides various performance requirements for support services [7], [8]. Also, the extension of the spectrum to the millimeter-wave (mmWave) bands led to a new system design that supports analog beamforming to warrant sufficient coverage, while conforming to the performance requirement of lower frequency bands. As different types of network configurations and channel models in different frequency bands must be considered, tremendous efforts are required for an individual or a development group to implement an SLS by its own efforts. Therefore, there is an on-going demand for an open-source system-level simulator that can develop and verify various 5G technologies, which creates a common platform to allows anyone to participate in the implementation and evaluation. However, the existing few open-source SLSs are not flexible enough to accommodate various operational features and new evaluation scenarios without a significant amount of reprogramming. Therefore, *5G K-SimSys* was developed as an SLS framework in a flexible, open, and modular (FOM) form [9]–[12].

To begin with, 5G K-SimSys is flexible as it can support various types of 5G environments and service scenarios. As an open-source software, this flexibility is further enriched by the participation of many researchers and developers. Second, 5G K-SimSys can be considered as one of the easy-to-design simulators due to its modularized and customizable structure. It can facilitate simulator modification and reconfiguration while integrating various algorithms under development in any evolving stages and unforeseen scenarios. This modular feature has been realized by building the elementary modules that can be reproduced or reused as hierarchically designed simulator objects.

5G K-SimSys is intended to be compatible with guidelines for evaluating radio interface technologies for IMT-2020 [7], which must be implemented for the evaluation of candidate technology submissions and for deciding on the qualifying RIT/SRIT technologies for 5G. It can be distinguished from the existing simulators [3], [13] by several factors. The Vienna system-level simulator in [3] is developed in MATLAB code. Even if it provides the key modules for SLS as an open sources, its flexibility is rather limited. The rigid modular structure is difficult to modify and extend to the additional objects. In other words, it would take enormous efforts to integrate a new object with different technical features into the existing structure. Meanwhile, the one in [13] is developed with open-source ns-3 simulator, integrating a full-stack mmWave module that can assess the end-to-end performance at the PHY layer and across all higher layers of the communication protocol stack for the 5G network. As it incurs inherent complexity of processing MAC and TCP layers in SLS, only a limited number of base and mobile stations can be considered. Therefore, dynamic conditions such as inter-cell interference cannot be immediately captured for more practical system-level performance assessment of multi-antenna technologies in cellular mobile systems.

The earlier design principles of 5G K-SimSys and its embodiments have been presented with a brief overview in [10] along with its application to evaluation of ultra-reliable & low latency communication in [11] and of massive MIMO [12]. Our objective in the current paper is to present how our SLS has been applied to evaluate the performance of 5G massive MIMO, while providing a comprehensive overview of 5G K-SimSys. This is a complete and self-contained version of presentation in the sense that it integrates new features and concepts while aggregating the key elements from recent developments. To this end, we present a complete review of 3GPP NR specification on massive MIMO, which was fully modeled for the current implementation. Furthermore, we propose a new beamforming scheme, referred to as bandwise analog beamforming (BAB), which is an innovative idea of handling the frequency selectivity issue to improve the performance of massive MIMO over the wideband operation. It will serve as an exemplary case that demonstrates how 5G K-SimSys can be employed to evaluate performance.

Massive MIMO is widely recognized as a key technology for improving the spectral efficiency in 5G [8], [14]–[17]. It is usually associated with a digital array of a large number (hundreds) of antenna elements serving much fewer UEs. With a large number of antennas, the channel vectors of multiple users tend to be nearly orthogonal with each other and thus, the effect of multi-user interference and thermal noise is largely reduced, allowing simple transmit or receive techniques. Three-dimensional (3D) massive MIMO/Full Dimension MIMO (FD-MIMO) configurations have been introduced in 3GPP by deploying active antenna elements in a two dimensional (2D) antenna array, which can dynamically control the beam direction toward a desired user [18]–[21]. In fact, digital arrays with a large number of antenna elements are made feasible owing to advances in active array antenna technology. Performance evaluation of massive MIMO systems requires intensive scheduling and interference calculations which involves complicated system models, including accurate 3D channel model, antenna configurations, feedback information, and multi-user scheduling algorithm. Meanwhile, massive MIMO also refers to analog beamforming with many antenna elements at mmWave band

which can fulfill the performance requirements for 5G, providing sufficient coverage against higher transmission loss.

The aforementioned technical features imply that a sophisticated means of evaluating the system-level performance is required for the massive MIMO-based 5G system. In fact, enormous efforts must be made to implement a system-level simulator for verifying the system efficiency or developing a specific algorithm for massive MIMO, subject to the various environments and system configurations. In this paper, we examine the 5G multi-antenna technologies in 3GPP NR specification, so as to develop the system-level model for 5G K-SimSys. One of our objectives is to discuss how new modules and other software structures can be implemented with 5G K-SimSys. Furthermore, we evaluate the performance of BAB, which requires a much more complex structure for system-level evaluation. Through these various embodiments, we demonstrate the flexibility and usefulness of 5G K-SimSys and how it can be employed for the advanced system design and optimization.

The remainder of this paper is organized as follows. Section II presents the massive MIMO system model, which includes analog beamforming and single/multi-panel digital beamforming based on the 3GPP NR specification. Section III presents actual implementation of 5G K-SimSys as a system-level simulator for massive MIMO, along with its overall platform architecture that aims to meet the open/modular/flexible design. Then, baseline simulation results are presented for various experiments. Section IV introduces the notion of bandwise analog beamforming and then, presents its implementation result, which demonstrates the modular and flexible features as a specific use case of 5G K-SimSys. Finally, conclusions are made in the last section.

II. GUIDELINES FOR MASSIVE MIMO: SYSTEM MODEL FOR 5G K-SimSys

Since multi-antenna techniques have been successfully introduced for improving spectral efficiency in LTE, they still play an essential role in 5G system design. In particular, mmWave band in 3GPP NR specification involves a beam-centric design to overcome higher transmission losses while providing sufficient coverage. To this end, analog beamforming is supported both at the gNB and UE, specifying beam management procedures. Furthermore, beamforming is also supported for initial access and broadcast signals in NR.

FD-MIMO/massive MIMO is also a beneficial technology at below 6 GHz frequencies for improving spectral efficiency. The underlying multi-antenna features developed in the later releases of LTE have been enhanced to further improve spectral efficiency for higher data rates and capacity over the limited spectrum. In [22], standardized FD-MIMO was reported for implementing elevation beamforming, and was later developed into an essential element of LTE-Advanced Pro (3GPP Rel-14), for 3D beamforming, i.e., beamforming in both horizontal and vertical dimensions. Both uplink feedback and downlink pilot overheads associated with a large number of antenna elements were reduced a smaller number of reference signals to consider only for an effective channel. Further, a transceiver unit (TXRU) has been introduced as a special interface for the active antenna system (AAS) to control the gain and phase of the individual antenna elements, by combining the features of a passive antenna element array with an active TXRU array. In addition, it involves various types of antenna configurations, e.g., 2D planar, to reduce the hardware complexity associated with a large number of antenna elements.

Meanwhile, NR aims at further improvements to increase the capacity with a major enhancement in a new flexible, modular, and scalable CSI framework [32]. It also includes a high-resolution CSI reporting mode to improve MU-MIMO operation. Furthermore, FD-MIMO/massive MIMO is considered an essential element of the systems operating in the above 6 GHz frequency range, e.g., mmWave band, since the high free-space path and penetration loss at those frequencies require large array gains to warrant sufficient signal-to-noise ratio (SNR), i.e., for sufficient coverage [23]. However, large antenna arrays increase the system complexity with conventional full digital beamforming having each antenna element connected to a separate radio frequency (RF) chain [24], [25]. In order to reduce its complexity, there have been efforts to find the optimal hybrid beamforming structure under various constraints for a given antenna configuration [26]–[30]. Furthermore, more flexible CSI acquisition and high-resolution feedback are specified in NR, along with a dual-stage codebook where a precoder is factorized into two components, one to capture the wideband channel properties and the other to capture the frequency selective part. This section presents an overview of massive MIMO specifications and their system models, focusing on the NR-specific features and functionalities as a basis for implementing 5G K-SimSys.

A. ANTENNA CONFIGURATION

In a digital array architecture, the antenna elements are arranged into 1-D linear array or 2-D planar array. Each antenna element is equipped with its own RF chain and analog-to-digital (AD) converter. Under a typical line-of-sight (LoS) channel in the mmWave band, many degrees of freedom may not be essential due to the fact that the benefits of frequency-selective digital precoding over analog beamforming are negligible. Therefore, a fully analog array architecture would be more acceptable for the LoS-dominant environments, e.g., in a small cell. In fact, to trade off the advantages and disadvantages of the fully digital and analog array architectures, a hybrid architecture has been considered earlier in the LTE specification. Inheriting the key structure of MIMO transmission over digital antenna ports, the standard has been extended to a hybrid beamforming structure with multi-panel arrays in NR. The structure establishes and maintains beam pairs for analog beamforming in both the BS and the UE for the mmWave band. As illustrated in Fig. 1, a 2D planar array can be divided into the rectangular

subarrays, referred to as panels, each of which is a uniform planar array. The panel arrays allow a partially connected hybrid architecture, which facilitates a simpler approach of designing the beamformers in an independent manner, i.e., one for each panel. Then, this particular architecture overcomes the difficulty of jointly designing the analog and digital beamformers, even if the channel at antenna element level cannot be independently considered due to the analog beamforming [22], [32].

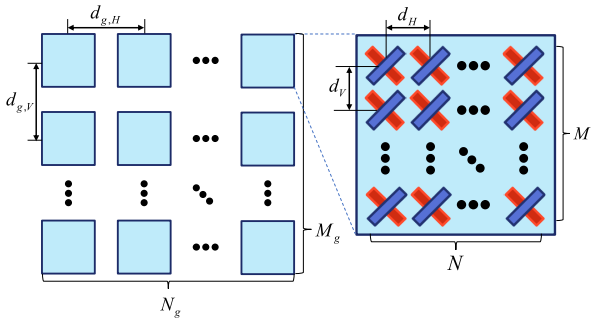

FIGURE 1. Configuration for panel antenna arrays [6].

We first consider a single panel array antenna in Fig. 1. It is an $M \times N$ uniform planar array with N antennas in each row and a total number of M rows in the vertical dimension with equal spacing. A larger planar array can be constructed with the multiple panels. Fig. 1 illustrates the antenna system that consist of M_g vertical and N_g horizontal antenna panels. Depending on vertical and horizontal panel spacing, the panel structures can be of two different types: a uniform antenna array and a non-uniform antenna array. Let d_H and d_V denote the distances between horizontal and vertical antenna elements in a panel, respectively. Furthermore, let $d_{g,H}$ and $d_{g,V}$ denote the distance between horizontal and vertical panels, respectively. In the uniform antenna array, the antenna elements of the same polarization are uniformly distributed across the whole panel array such that there is no explicit spacing to differentiate the adjacent antenna elements from different antenna panels, e.g., $\left(d_{g,H}, d_{g,V}\right) = ((M-1)d_H, (N-1)d_V)$ in Fig. 1. On the contrary, in the non-uniform antenna array, the space between adjacent antenna elements in adjacent panels is different from that within the panels, e.g., $\left(d_{g,H}, d_{g,V}\right) \succ ((M-1)d_H, (N-1)d_V)$ in Fig. 1 [33].

The above antenna configuration arranges the transmit signals as virtual beams to support the MU-MIMO in 3D, i.e., serving multiple users on the same bandwidth simultaneously in full dimension. The antenna configuration is denoted by $\left(M, N, P, M_g, N_g\right)$, where P is the number of polarization dimensions, e.g., $P = 2$ for cross-polarization (X-pol). Then, the total number of antenna elements is given by $MNPM_gN_g$. Even though a uniform linear antenna is more appropriate for MU-MIMO than $P = 2$, subject to the same number of antenna elements [34], X-pol allows for enhanced capacity with more antenna elements within the limited physical space, as typically practiced in 5G systems. In the current system under consideration, we set the cross-polarization angles to (0°, 90°) and ±45° in the UE and gNB, respectively.

B. HYBRID BEAMFORMING FOR 2D AAS

A baseband precoder processes the output of the layer mapper, which will be distributed to antenna ports. An antenna port is defined as a logical element to which a reference signal is assigned for channel state information, channel estimation for demodulation, sounding signal, etc, in the 3GPP specification. A single physical antenna can belong to multiple antenna ports, whose effective channels are different, e.g., two signals on the same physical antenna carrying different beamforming weights. In the specification, there are various types of reference signals, e.g., a channel state information reference signal (CSI-RS), demodulation reference signal (DMRS), phase tracking reference signal (PTRS), and sounding reference signal (SRS), that are the transmitted reference signals assigned to antenna ports. Hence, the antenna port can be defined by the transmitted reference signal. Meanwhile, a TXRU is a special interface for AAS, having power amplifier (PA) and low noise amplifier (LNA), so that gNB can control the gain and phase of the individual antenna element. It establishes a hardware connection between the baseband signal path and antenna array elements via a radio distribution network, which delivers the transmit signal from PA to antenna elements, and receive signals from antenna elements to LNA. As opposed to a fully digital array which has an RF chain and a data converter for each antenna element, it combines large-dimensional analog pre/postprocessing with lower-dimensional digital processing and thus, a much lower number of active antenna elements are employed which reduces the power consumption and hardware cost [20]. When implementing a 2D AAS in an FD-MIMO architecture, the radio resource comprises of antenna ports, TXRUs, and physical antenna elements. A data stream on an antenna port is precoded on TXRUs in the digital domain, which is a process referred to as antenna port virtualization (port-to-TXRUs mapping). Considering one-to-one mapping between ports and TXRUs allows for both terms to be used interchangeably.

The signal on a TXRU is precoded by phase shifts or variable gain amplifiers on a group of physical antenna elements in the analog domain. This process, referred to as TXRU virtualization, defines a mapping of TXRUs signals to those of the antenna elements. In other words, TXRU virtualization allows for a group of antenna elements to be configured for transmitting or receiving the same data. From the end-to-end design point, in the transmitter, hybrid beamforming can be modeled as antenna port and TXRU virtualizations to deal with analog and digital domain signals, respectively. In other words, it combines digital precoding of the transmission layers into antenna ports and then analog precoding of the antenna ports into physical antennas. This process requires the channel estimation only for each antenna

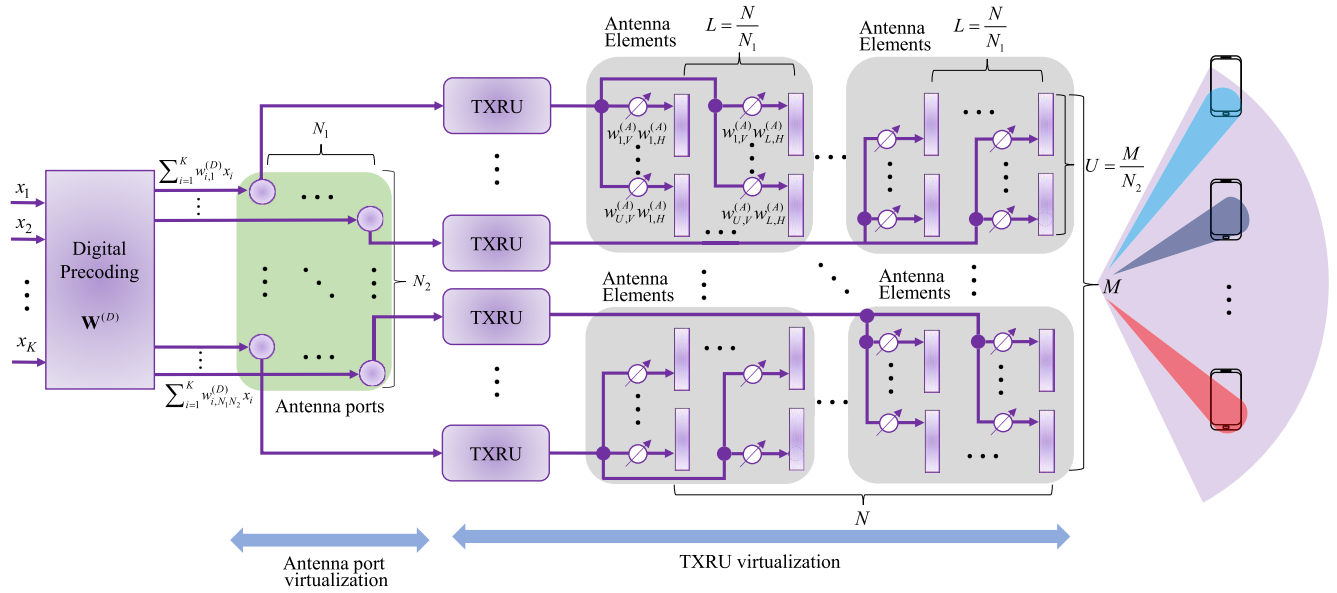

(a) Non-precoded CSI-RS

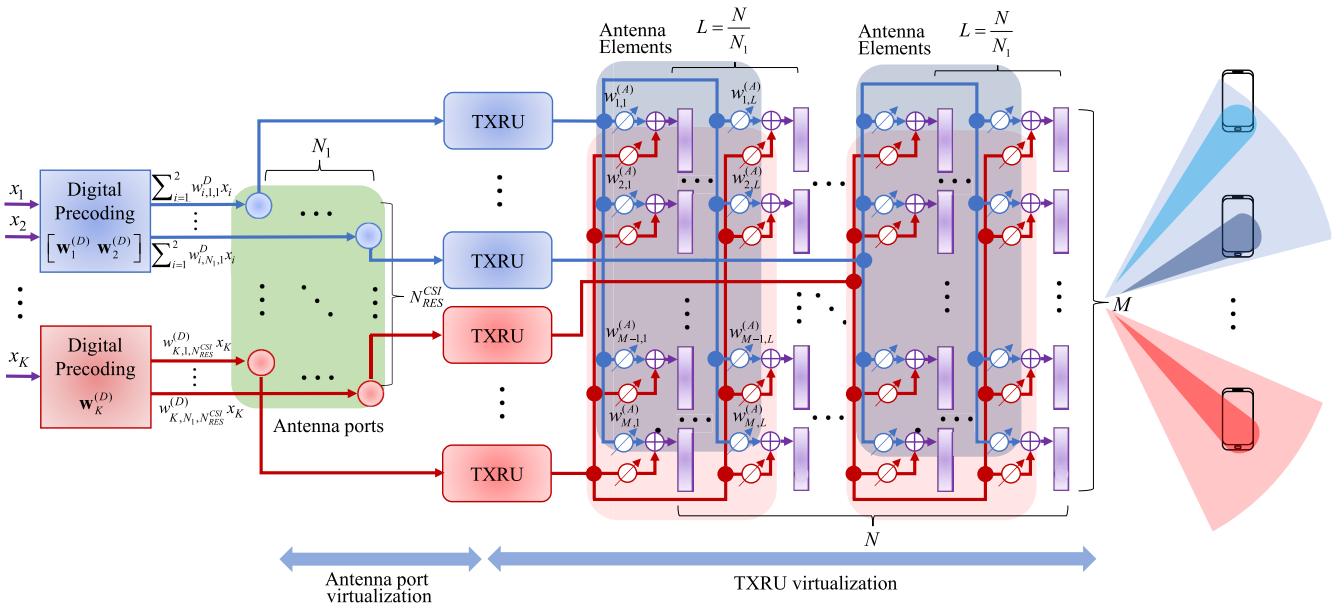

(b) Beamformed CSI-RS

FIGURE 2. **CSI-RS transmission type for hybrid beamforming: Illustrative structures ($P = 1$).**

port, rather than channel estimation for all $MNPM_gN_g$ physical antenna elements.

The downlink transmit signals is represented by $\mathbf{x} = [x_1, x_2, \cdots x_K]^T$ with covariance of $\sum = \mathbb{E}\left[\mathbf{x}\mathbf{x}^H\right]$, where x_i denotes the transmit signal for UE i, for corresponding modulation symbol, e.g., QPSK, 16-QAM, or 64-QAM, depending on modulation and coding set (MCS). Let $\mathbf{H}$ denote a channel matrix of a rank of K, with each element to represent a complex channel gain between each Tx and Rx antennas. In the hybrid beamforming structure, the received signals, denoted by K-dimensional vector $\mathbf{y}$, for the K scheduled UEs, each with a sinlge antenna element are given as follows:

$$\mathbf{y} = \mathbf{H}\mathbf{W}^{(A)}\mathbf{W}^{(D)}\mathbf{x} + \mathbf{n}. \tag{1}$$

where $\mathbf{W}^{(A)}$ and $\mathbf{W}^{(D)}$ represent analog and digital precoding matrices, respectively. Meanwhile, $\mathbf{n}$ denotes the Gaussian noise, including inter-cell interference with an average power of σ_n^2 in a multi-cell scenario.

Depending on the configuration of the antenna ports of the physical antenna elements, there are two different TXRU structures for hybrid beamforming. One is an array partitioning structure, in which the antenna elements are divided into multiple groups. Each group of antenna elements

is connected to one TXRU while orthogonal CSI-RSs are assigned to each group. As each TXRU transmits its CSI-RS, the UE can measure the channel from the non-precoded CSI-RS of all TXRUs. The other is an array connected structure in which output signals of multiple TXRUs are delivered to the single antenna element while orthogonal CSI-RSs are assigned to each TXRU. As the multiple TXRUs share a group of antennas, each CSI-RS is precoded with different weights, allowing the UE to measure the precoded channel from the beamformed CSI-RS. Non-precoded CSI-RS and beamformed CSI-RS are the two possible implementation practices that have been introduced in LTE Rel-13. Even if non-precoded CSI-RS and beamformed CSI-RS are not explicitly referred to in NR, they are considered as two possible implementation practices for system-level evaluation of massive MIMO. Fig. 2 illustrates two different TXRU structures for hybrid beamforming, one with nonprecoded CSI-RS transmission for the array partitioning structure and the other with beamformed CSI-RS transmission for the array connected structure. In the sequel, we give details for these two TXRU structures, in which an $M \times N$ uniform planar array is considered.

1) ARRAY PARTITIONING STRUCTURE WITH NON-PRECODED CSI-RS TRANSMISSION

As illustrated in Fig. 2(a), N horizontal and M vertical antenna elements are mapped into PN_1 and N_2 antenna ports by partitioning them into multiple groups, each with L horizontal and U vertical elements. Each antenna port is fully connected to all physical antenna elements within the corresponding partitioned group, creating a partitioned antenna array, represented as an analog precoding matrix $\mathbf{W}^{(A)} \in \mathbb{C}^{MNP \times N_1 N_2 P}$. By denoting the vertical and horizontal weights as $\mathbf{w}_V^{(A)} = [w_{1,V}^{(A)}, w_{2,V}^{(A)} \cdots w_{U,V}^{(A)}]$ and $\mathbf{w}_H^{(A)} = [w_{1,H}^{(A)}, w_{2,H}^{(A)} \cdots w_{L,H}^{(A)}]$, respectively, the analog precoding matrix is given by the Kronecker product $\mathbf{W}^{(A)} = \mathbf{w}_V^{(A)} \otimes \mathbf{w}_H^{(A)}$. Even if it is not specifically provided in the NR specification, the following setting is employed in our implementation:

$$w_{u,V}^{(A)} = \frac{1}{\sqrt{U}} \exp\left(-j\frac{2\pi}{\lambda}(u-1)d_V \cos\theta_V\right), \quad u = 1, 2, \cdots, U \tag{2}$$

$$w_{l,H}^{(A)} = \frac{1}{\sqrt{L}} \exp\left(-j\frac{2\pi}{\lambda}(l-1)d_H \sin\theta_H\right), \quad l = 1, 2, \cdots, L \tag{3}$$

where λ is the wavelength, and θ_V and θ_H are the tilting angles for vertical and horizontal antennas, respectively [22]. Note that beamwidth of the analog beam is governed by U and L, i.e., more antenna elements leading to a sharper beam. In this configuration, channels are estimated for $N_1 N_2 P$ antenna ports using the CSI-RS, one for each port, in the receiver.

In Fig. 2(a), $\{w_{i,j}^{(D)}\}_{j=1}^{N_1 N_2 P}$ denotes the digital precoder for UE i, selected using the feedback information from all UEs. The codebooks for digital precoding in the 3GPP specification are presented in the following subsection. Each antenna port is allocated to the different antenna elements. As it does not require any precoding to differentiate one port from the other on the same antenna, this particular type of hybrid beamforming is referred to as *non-precoded* CSI-RS transmission.

2) ARRAY CONNECTED STRUCTURE WITH BEAMFORMED CSI-RS TRANSMISSION

A separate set of antenna ports can be configured for a group of UEs that employ the same analog beam while fully connecting each antenna port with the physical antenna elements within the partitioned set. Furthermore, different user signals can be transmitted using the same physical antenna that corresponds to the different antenna ports if they are beamformed with the different analog precoders. Let $\{w_{i,j,q}^{(D)}\}_{j=1}^{N_1 P}$ denote a digital precoder for UE i in group q. The precoded symbols for each UE are mapped to the set of antenna ports for each group. More specifically, Fig. 2(b) illustrates two UEs, namely UE 1 and UE 2, in the same analog beam, each of which is digitally precoded by $\{w_{i,j,q}^{(D)}\}$ for $i = 1$ and 2. A total number of N_{RES}^{CSI} beams are generated with the analog precoding matrix $\mathbf{W}^{(A)} \in \mathbb{C}^{N_1 N_{RES}^{CSI} \times MNP}$, allocating MNP/N_{RES}^{CSI} antenna ports to each beam. The N_{RES}^{CSI} CSI-RS resources, each associated with a single analog beam, are available over each time to interval (TTI). If we denote the precoding matrix for beam q as $\mathbf{W}_{(q)}^{(A)}$, the overall analog precoding matrix can given by $\mathbf{W}^{(A)} = \left[\mathbf{W}_{(1)}^{(A)}, \mathbf{W}_{(2)}^{(A)}, \cdots, \mathbf{W}_{(N_{RES}^{CSI})}^{(A)}\right]^T$. Similar to (2) and (3), the analog precoding matrix $\mathbf{W}_{(q)}^{(A)}$ in the current implementation is set as

$$w_{q,m,l}^{(A)} = \frac{1}{\sqrt{ML}} \exp\left(-j\frac{2\pi}{\lambda}(m-1)d_V cos\,\theta_{q,V}\right) \cdot \exp\left(-j\frac{2\pi}{\lambda}(l-1)d_H \sin\theta_{q,H}\right), \quad m \in (1, 2, \cdots, M),\ l \in (1, 2, \cdots, L) \tag{4}$$

where $\theta_{q,V}$ and $\theta_{q,H}$ are the tilting angles for vertical and horizontal antennas, respectively, for beam q [22]. Note that (4) is a generalized expression for when analog beamforming is applied to both vertical and horizontal planes. Because more antenna elements are connected to the antenna port associated with each beam, the beamformed CSI-RS type can generate sharper beams than the non-precoded CSI-RS type (while scaling the beam power by N_{RES}^{CSI}). For selecting the best beam, each UE receives the reference signals with different beams over N_{RES}^{CSI} CSI-RS resources and then measures the reference signal received power (RSRP). Then, the best RSRP is determined, and its beam index known as a CSI-RS Resource Indicator (CRI) is reported together with RSRP and CSI sets that indicate the channel quality and other channel properties in terms of Channel Quality Indicator (CQI), Precoding Matrix Indicator (PMI), and Rank Indicator (RI).

The hybrid beamforming structure with all the above features in the LTE specification, more specifically based upon the later releases, i.e., 3GPP Rel-13 and Rel-14, is still maintained in the NR specification while a high-resolution CSI reporting is included for improved MU-MIMO operation. The following subsection presents the detailed enhancement for digital beamforming with high-resolution CSI, based on the dual-stage codebooks. Furthermore, beam management is discussed in a separate subsection.

C. DIGITAL BEAMFORMING

As opposed to employing both codebook-based and non-codebook-based schemes for MIMO transmission in LTE, NR is mainly based on only non-codebook-based precoding for MIMO while employing CSI-RS and DMRS for CSI acquisition and coherent demodulation, respectively. As discussed in Section II.B, CSI must be estimated and reported for each port, in the downlink feedback-based CSI acquisition at the transmitter. In fact, it is the quantized CSI in the form of CQI, PMI, RI, and CRI. For example, codebook-based CSI acquisition is used for each UE, to evaluate which precoding matrix in the codebook would give the best performance if used by the BS [32] and to feed back the corresponding PMI. It is critical to reduce the feedback overhead and CSI complexity for the codebook-based CSI, especially when the number of antennas port increases. To this end, several codebooks in the LTE and NR are designed to exploit a correlation between antenna ports for closely spaced antenna elements with limited angular spread.

As opposed to the LTE-Advanced Pro which specifies only a single-panel codebook, NR includes four different PMI types, depending on the number of panels and codebook types, namely 'Type I single-panel', 'Type I multi-panel', 'Type II', and 'Type II port selection'. The 3GPP standard has specified a double codebook that supports the X-pol antenna in Release 10 and beyond. Here, the DFT matrix and phase difference between cross-polarizations are sufficient to specify the codebook with 2D-DFT. However, representing the precise CSI might be challenging when the number of generated DFT vectors is limited by the number of antenna ports. Therefore, to improve the accuracy, DFT vectors are oversampled with the factors $O_i,\ i = 1, 2$, in LTE-Advanced Pro and NR specifications.

As in the codebook with 2D-DFT, the panel-based codebook can be specified by the phase difference from the reference panel. As opposed to Type I codebook that selects only one oversampled DFT vector, Type II codebook selects a set of beams, where the quantized amplitudes are controlled by the power per each path, involving more feedback overhead than Type I codebook. Finally, 'Type II port selection' codebook is a beamformed CSI-RS version of Type II codebook, applied to a specific antenna port.

In this study, we consider only the rank 1 'Type I' codebook, which has the following panel precoding matrix

TABLE 1. Antenna port configurations [32].

N_1N_2P	(N_1, N_2)	(O_1, O_2)
4	(1,2)	(4,4)
	(2,1)	(4,1)
8	(2,2)	(4,4)
	(4,1)	(4,1)
16	(4,2)	(4,4)
	(8,1)	(4,1)
32	(8,2)	(4,4)
	(16,1)	(4,1)

TABLE 2. 'Type I single panel' codebook [32].

i_2	0	1	2	3
precoder	$\mathbf{W}^{(1)}_{l,m,0}$	$\mathbf{W}^{(1)}_{l,m,1}$	$\mathbf{W}^{(1)}_{l,m,2}$	$\mathbf{W}^{(1)}_{l,m,3}$
i_2	0	1	2	3
precoder	$\mathbf{W}^{(1)}_{l+1,m,0}$	$\mathbf{W}^{(1)}_{l+1,m,1}$	$\mathbf{W}^{(1)}_{l+1,m,2}$	$\mathbf{W}^{(1)}_{l+1,m,3}$
i_2	0	1	2	3
precoder	$\mathbf{W}^{(1)}_{l+2,m,0}$	$\mathbf{W}^{(1)}_{l+2,m,1}$	$\mathbf{W}^{(1)}_{l+2,m,2}$	$\mathbf{W}^{(1)}_{l+2,m,3}$
i_2	0	1	2	3
precoder	$\mathbf{W}^{(1)}_{l+3,m,0}$	$\mathbf{W}^{(1)}_{l+3,m,1}$	$\mathbf{W}^{(1)}_{l+3,m,2}$	$\mathbf{W}^{(1)}_{l+3,m,3}$
i_2	16-31			
precoder	Replace the second subscript m with $m+1$ in 0-15			

with 2D-DFT:

$$\mathbf{W}^{(D)} = \mathbf{W}^{(1)}_{\underbrace{s_1 i_{1,1}}_{l},\underbrace{s_2 i_{1,2}}_{m},n} = \frac{1}{\sqrt{N_1N_2P}} \begin{bmatrix} v_{l,m} \\ \phi_n v_{l,m} \end{bmatrix}. \tag{5}$$

where $\phi_n = e^{j\pi n/2}$ where $n = 0, 1, 2, 3$ is the cross-polarized phase difference and $v_{l,m}$ denotes the element of oversampled DFT matrix with the oversampling factor of O_1 and O_2, representing the channel direction for reference polarization, given as follows:

$$v_{l,m} = \begin{bmatrix} u_m & e^{j\frac{2\pi l}{N_1O_1}} u_m & \dots & e^{j\frac{2\pi l(N_1-1)}{N_1O_1}} u_m \end{bmatrix}^T \tag{6}$$

where

$$u_m = \begin{cases} \begin{bmatrix} 1 & e^{j\frac{2\pi m}{N_2O_2}} & \dots & e^{j\frac{2\pi m(N_2-1)}{N_2O_2}} \end{bmatrix}, & N_2 > 1 \\ 1, & N_2 = 1 \end{cases} \tag{7}$$

Note that s_1 and s_2 in (5) are used to select the codebook subset. The antenna configurations for 'Type I single panel' codebook is given by Table 2. Each UE selects the optimal precoding matrix given by (5). The selected matrix will be reported with the index values, $i_1 = \left[i_{1,1}, i_{1,2}\right]$ and i_2, which determines the codebook as defined in Table 2. ''Type I'' codebook has two codebook modes, codebookMode = 1 and 2, depending on feedback overhead. Note that codebookMode = 2 follows Table 2 considering $i_2 \in (0, 15)$ while taking the more DFT subsets than codebookMode = 1 with $i_2 = 0, 1, 2, 3$. See [31] for codebooks for other rank or codebookMode.

For multiple panels in NR, digital precoding is considered only for one-dimensional antenna ports. Therefore, although not expressed in the standard specification, the mentioned consideration should be met for determining the analog beam. Multi-panel digital precoding needs to be performed on the effective channel projected onto the vertical panel.

In addition, for $N_g = 2$ or 4, horizontal panels are supported. In 'Type I Multi Panel' codebooks, codebookMode is also used for inter-panel correction updates [32]. When codebookMode = 1, it is similar to the concept of digital precoding for 'Type 1 single-panel'. The DFT coefficient of digital precoding for 'Type 1 multi-panel' is determined by phase relationship between the two antenna panels. More specifically, referring to $\mathbf{W}^{(1)}_{l,m,n}$ in (5) as a reference single panel, precoding matrices for the remaining panels are determined by the inter-panel co-phasing factor φ_k, which reflects the panel correlation with the reference panel. The precoding matrix $\mathbf{W}^{(D)}$ for multi-panel antenna is then given as

$$\mathbf{W}^{(D)} = \begin{bmatrix} \mathbf{W}^{(1)}_{l,m,n} & \varphi_k \mathbf{W}^{(1)}_{l,m,n} \end{bmatrix}^T = \frac{\begin{bmatrix} v_{l,m} & \phi_n v_{l,m} & \varphi_k v_{l,m} & \varphi_k \phi_n v_{l,m} \end{bmatrix}^T}{\sqrt{N_1 N_2 P}} \tag{8}$$

where $\varphi_k = e^{j\pi k/2}$ with $k = 0, 1, 2, 3$. codebookMode = 1 is available when $N_g = 2$ or 4. In contrast, codebookMode = 2 is supported only when $N_g = 2$. By updating of the phase relationship between panels and phase difference between cross-polarization, the matrix can be expressed as

$$\mathbf{W}^{(D)} = \frac{\begin{bmatrix} v_{l,m} & \phi_n v_{l,m} & a_{p_1} b_{n_1} v_{l,m} & a_{p_2} b_{n_2} v_{l,m} \end{bmatrix}^T}{\sqrt{N_1 N_2 P}} \tag{9}$$

where $a_p = e^{j\pi(2p+1)/4}$ and $b_n = e^{j\pi(2n-1)/4}$.

D. ANALOG BEAM MANAGEMENT

As channel conditions can be more vulnerable to mobility or blockage for much sharper and more beams in the mmWave band, beam management has been introduced in NR for efficient analog beamforming. It is defined as a set of procedures for layers 1 and 2 to acquire and maintain a set of BS and UE beams, including features such as beam sweeping, beam measurement, beam reporting, beam determination, beam maintenance, and beam recovery. Two different reference signals are used for downlink beam management: synchronization signal block (SSB) and CSI-RS. SSB consists of synchronization signals and physical broadcast channel (PBCH). As opposed to a block of synchronization signal and PBCH in LTE that has fixed time-domain and frequency-domain positions in every subframe, SSB transmits signals in various patterns, depending on subcarrier spacing and some other parameters. Furthermore, a set of multiple SSBs is defined as an SS burst set, which is repeated with a given periodicity, e.g., 20 ms. The multiple SSBs in a SS burst set are then transmitted repeatedly in different beams, allowing the UE to measure the different SSBs to determine the best BS transmit beam during an initialization phase. The maximum number of SSBs within a SSB set, denoted by $L_{\max}$, is specified in NR, i.e., $L_{\max} = 4$ or 8 in sub 6 GHz and $L_{\max} = 64$ in mmWave band.

Three different types of beam sweeping processes, P1 for initial transmit/receive beam selection, P2 for BS transmit beam change, and P3 for UE receive beam change, have been defined in radio resource control connected state. For example, the BS performs a beam sweep over an angular sector that covers the entire cell by transmitting a unique reference signal in each beam (P1), which are relatively wide to limit the number of beams to sweep. Then, a beam can be refined by performing a beam sweep over a narrower angular sector around the best beam reported by the UE. Narrowing the range allows the UE to detect the best one and report it to BS (P2). UE refines its receiver beam by repeatedly using a fixed beam transmitted by the BS, where beam pairs are established for analog beamforming in both the BS and UE (P3).

Beam maintenance is required to deal with beam misalignment. More specifically, beam tracking and refinement is implemented so that a beam can be switched to another beam with better quality. Beam recovery is required to find a new beam if a communication link cannot be maintained with the current beam. Beam measurement measures the quality of different beams on SSB or CSI-RS transmitted by the BS. There are two different types of beam reporting, both indicating the best beams along with their measured qualities: grouping-based reporting and nongrouping-based reporting. In grouping-based reporting, a group of BS Tx beams can be received simultaneously by the UE, allowing the establishment of links between multiple beam pairs. However, in nongrouping-based reporting, the UE is configured to sweep the multiple beams individually and report up to four beams. Due to its robustness, the grouping-based reporting has been shown to outperform the nongrouping-based reporting by approximately 15% [35]. However, this study considers only the nongrouping-based reporting.

III. 5G K-SimSys FOR MASSIVE MIMO: IMPLEMENTATION & PERFORMANCE ANALYSIS

The 5G K-SimSys was designed and implemented to provide an open platform and testbed for evaluating the system-level performance of 5G standard [9]–[12]. One of the key features in 5G K-SimSys is its modular and flexible structure that allows the reuse of the same modules for various system configurations by modifying existing or including additional modules for newly introduced algorithms and/or functionalities. Furthermore, it will be open to public so that all its modules can be redesigned and shared for research and development in 5G system.[1] It should be noted that implementation of massive MIMO, especially conforming to the current 5G standard specification, involves many existing key modules in 5G K-SimSys.

Fig. 3 illustrates the overall modular structure of the 5G K-SimSys having five key functionality layers: `Simulation Top`, `Network Configuration`, `Channel Model`, `Radio Resource Management`, and `Link Performance` [9]–[12]. Furthermore, the functionalities in an individual layer are executed by three

[1]The current version of 5G K-SimSys is available at https://github.com/5GKSimSys/5G-K-SimSys

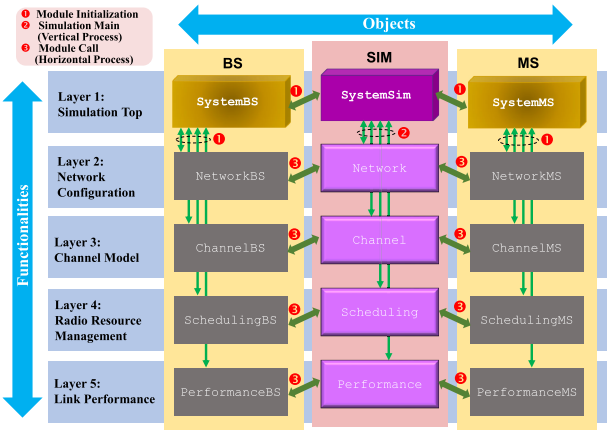

FIGURE 3. Main modules in 5G K-SimSys.

different entities, each referred to as an "object." The *object* **SIM** is a main entity that defines and triggers overall simulation processes for all modules in the different layers. Every object inherits the same functional layer structures. A specific functionality in each layer is triggered by the *object* **SIM**, and the actual execution is completed by the other two entities, *object* **MS** and *object* **BS**. Depending on the functional requirements and performance indicators, additional classes of objects can be defined and integrated. For example, two different classes of *object* **MS** can be defined when eMBB and uRLLC devices coexist with the different performance indicators, e.g., *object* **MSeMBB** for eMBB devices and *object* **MSuRLLC** for uRLLC devices [10]. The current modular and flexible structure immediately facilitates extension of the baseline simulator to various scenarios and functional requirements.

Individual functionality in each layer of the different object is embodied by a module, which implements the detailed procedures and stores data generated through the simulation. Its function and data are identified by the corresponding object which facilitates the retrieval [9]–[12]. **Simulation Top** is the highest layer that integrates the overall simulation processes and manages the entire flow of simulation by triggering individual functionalities in the lower layers of each object. However, only three modules, `SystemSim`, `SystemBS`, and `SystemMS` are transparent in this layer, abstracting the specific functionalities in the lower layers. Therefore, the readability of the entire simulator can be improved.

The module `SystemSim` executes the simulation process by calling up the modules in the lower layers (vertical processing), which subsequently calls up the corresponding modules in the same layer of module `SystemBS` and/or module `SystemMS` (horizontal processing). Furthermore, **Simulation Top** layer directly interacts with all modules in the lower layers for initialization.

Fig. 4 illustrates an embodiment of module `SystemSim`, which interacts with all other modules in the lower layers of the baseline 5G K-SimSys. Furthermore, each module is

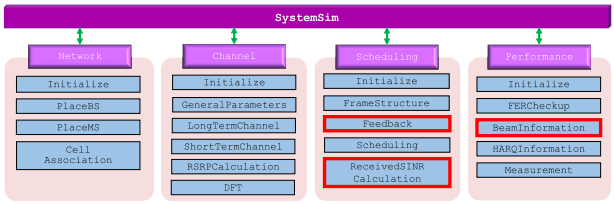

FIGURE 4. Overall simulator structure: Sub-modules.

embodied by submodules, which are the lower functional blocks that implement the detailed simulation process. The submodules can be added or reset according to the simulation scenario. In this section, we discuss how the modular and flexible feature of 5G K-SimSys can immediately extend the current baseline simulator to implement 5G massive MIMO for NR (NR-MIMO), which is analyzed in Section II.

A. IMPLEMENTATION

The submodules with black-line box are the basic modules that do not change in the different entity object. Meanwhile, SLS for NR-MIMO involves modification of only several submodules, indicated by the red-line boxes in Fig. 5. They include submodules of `Feedback` and `ReceivedSINRCalculation` in `Scheduling` module and `BeamInformation` in `Performance` module.

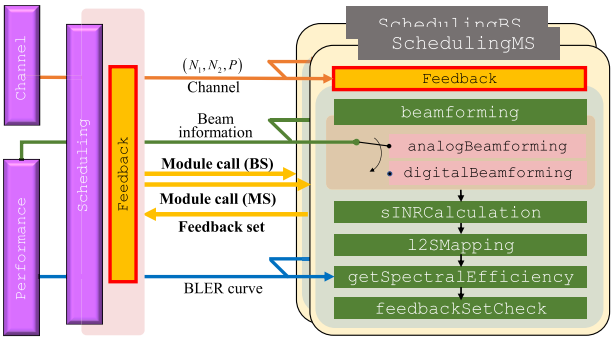

FIGURE 5. 5G K-SimSys: Feedback module for NR-MIMO.

The module `Scheduling` involves a timely interaction between gNB and UE, achieved by invoking the submodule `Feedback` for feedback information. A feedback set (CQI, PMI, RI, and CRI) is determined upon each module call as the output of submodule `Feedback`. Fig. 5 presents detailed implementation of the submodule `Feedback` that interacts with module `Scheduling`. Note that all submodules in each module are controlled by a main object **SIM** that merely triggers the corresponding modules in objects **MS** and **BS**. For example, the submodule `Feedback` in the module `Scheduling` triggers a `Feedback` submodule that will be executed by object `SchedulingBS` or `SchedulingMS`, depending on the entity indicated by the module call input. The function `beamforming`

is a key element of submodule `Feedback` in which a link performance is mainly governed by the beamforming gain. The antenna configuration of (N_1, N_2, P), channel for each UE, and beam information are initialized as input to the function `beamforming`. Note that two types of CSI-RS transmissions are supported for hybrid beamforming, as analyzed in Section II. The configurations with $N_2 = 1$ and $N_2 > 1$ correspond to beamformed CSI-RS and nonprecoded CSI-RS types, respectively. As shown in Fig. 4, the submodule `BeamInformation` triggers either function `beamMaintenance` or function `beamRecovery` with two-bit indicator. The function `analogBeamforming` is required if one of the two bits is indicated as '1' during performance measurement. In the case of beam maintenance, the first bit of beam information becomes '1' when RSRP of the selected beam drops more than twice. In addition, the current implementation limits the maximum number of HARQ retransmissions to four, after which a link failure is declared. Beam refinement is executed until two consecutive HARQ retransmissions fail. During beam recovery, if more than two consecutive HARQ retransmissions fail, the second beam information is set to '1'. Beam sweeping searches for an analog beam pair, which is an essential part of the initial access procedure. Toward this end, as the function `analogBeamforming` must be called, two-bit indicator of beam information is initialized as '11'. If at least one of two bits is set to '1', it is updated as '00' after beam determination. If beam information indicates '00' at the time of calling the submodule `Feedback`, it implies that the previously selected analog beam works, i.e., only a function `digitalBeamforming` is executed without invoking the function `analogBeamforming`. Each UE then stores the best analog beam sets that have been selected for the given CSI-RS transmission type.

In the function `digitalBeamforming`, PMI that maximizes the signal-to-leakage and noise ratio (SLNR) is selected for 'Type I single-panel' codebook in Table 1 or 'Type I multi-panel' codebook for multi-panel case. For each UE, a maximum of 8 layers can be supported for SU-MIMO. Once PMI is determined, SINR of each subcarrier is calculated using the function `sINRCalculation`. Then, the effective SINR is calculated by the `l2SMapping` function, in which the frequency-domain channel and interference are taken into account for measuring the received signal strength.

The link-to-system (L2S) mapping, e.g., mutual information-based exponential SNR mapping (MIESM), is also an essential part of calculating the effective SINR, and can be replaced with other L2S mapping methods to capture the specific characteristics. An effective SINR is computed to identify CQI from BLER curve, which is obtained by LLS over the additive white Gaussian channel, as described in the SLS methodology [1]–[5]. Afterwards, CQI, PMI, and RI are fed back by UE. For the case of $N_2 = 1$, i.e., beamformed CSI-RS type, CRI stored in the function `analogBeamforming` is also reported. Based on the CQI/PMI/RI/CRIs and RSRPs for the reported CRIs by all UEs, the `Scheduling` module determines the set of UEs to be served simultaneously for MU-MIMO. It considers a possible spatial multiplexing gain in terms of the number of layers for each UE. Different algorithms, including the proportional fair (PF) algorithm, can be introduced for multi-user scheduling [33]. Towards this end, an active set of UEs that require HARQ must be considered, along with the scheduled UEs. Because the specific scheduling algorithm is not a rigid part of 5G K-SimSys, existing algorithms can be modified or replaced in a flexible and modular manner.

Similarly, the submodule `ReceivedSINRCalculation` in the Module `Scheduling` triggers the peer submodule `ReceivedSINRCalculation` in module `SchedulingBS` or `SchedulingMS`, for calculating the received SINR of the UEs that are scheduled over TTI, based on their beamforming information. This particular submodule reuses `sINRCalculation` and `l2SMapping` functions in the submodule `Feedback`. The effective received SINR is computed by (11) and returned to submodule `ReceivedSINRCalculation` in the module `Scheduling` using the effective estimated channel via DMRS. Let S_ℓ denote a set of UEs that are scheduled for MU-MIMO transmission in BS ℓ, $\ell \in C$, where C denotes a set of BS's. Without loss of generality, we consider a single data stream per user. Let $\mathbf{H}_{\ell,k}$ denote a MIMO channel matrix between BS ℓ and UE k. Furthermore, let $\mathbf{W}_\ell^{(A)} = \left[\mathbf{W}_{\ell,1}^{(A)}, \ldots, \mathbf{W}_{\ell,|S_\ell|}^{(A)}\right]^T$ and $\mathbf{W}_\ell^{(D)} = \left[\mathbf{W}_{\ell,1}^{(D)}, \ldots, \mathbf{W}_{\ell,|S_\ell|}^{(D)}\right]^T$ represent the analog and digital precoding matrices in BS ℓ, respectively. Assuming equal power allocation to all users served by the given gNB with transmit power of P, i.e., $tr\left(\sum\right) = \frac{P}{|S_\ell|}\mathbf{I}_k$, the received signal for UE is given as

$$\begin{aligned}\mathbf{y}_{\ell,k} &= \sqrt{P/|S_\ell|}\cdot\begin{pmatrix}\mathbf{H}_{\ell,k}\mathbf{W}_{\ell,u}^{(A)}\mathbf{W}_{\ell,k}^{(D)}x_{\ell,k}\\ +\sum_{j\in S_\ell\setminus k}\mathbf{H}_{\ell,k}\mathbf{W}_{\ell,j}^{(A)}\mathbf{W}_{\ell,j}^{(D)}x_{\ell,j}\end{pmatrix}\\ &\quad+\sum\nolimits_{c\in C\setminus\ell}\sqrt{P/|S_c|}\cdot\mathbf{H}_{c,k}\mathbf{W}_c^{(A)}\mathbf{W}_c^{(D)}\mathbf{x}_c+\mathbf{n}_{\ell,k}\end{aligned}\tag{10}$$

where $x_{\ell,k}$ and $\mathbf{n}_{\ell,k}$ denote the transmitted symbol and the additive white Gaussian noise for UE k in BS ℓ, respectively. Assuming that a minimum mean square error-interference rejection combining (MMSE-IRC) filter $\mathbf{g}_{\ell,k}$ is employed in the receiver for UE k in BS ℓ, the SINR for UE k in BS ℓ is represented as

$$\gamma_{\ell,k} = \frac{\left|\mathbf{g}_{\ell,k}\mathbf{H}_{\ell,k}\mathbf{W}_{\ell,k}^{(A)}\mathbf{W}_{\ell,k}^{(D)}\right|^2}{|S_\ell|\,\sigma_{\ell,k}^2+\left\|\mathbf{g}_k\begin{pmatrix}\mathbf{H}_{\ell,k}\mathbf{W}_{\ell,-k}^{(A)}\mathbf{W}_{\ell,-k}^{(D)}\\ +\sum_{c\in C\setminus\ell}\mathbf{H}_{c,k}\mathbf{W}_c^{(A)}\mathbf{W}_c^{(D)}\end{pmatrix}\right\|_F^2}\tag{11}$$

where $\sigma_{\ell,k}^2 = \left|\mathbf{g}_{\ell,k}\right|^2\sigma_n^2/P$ while $\mathbf{W}_{-k}^{(A)}$ and $\mathbf{W}_{-k}^{(D)}$ denote precoding matrices for analog and digital beamforming that

TABLE 3. Simulation models and parameters.

Model/Parameters			Value
Channel model	Spatial channel model		3GPP TR 38.901 [6]
	Noise power spectral density (N_0)		$N_0 = -174dBm/Hz$
	Antenna pattern	3dB bandwidth (θ_{3dB}, ϕ_{3dB})	$\theta_{3dB} = 65^\circ$ $\phi_{3dB} = 65^\circ$
		Side-lode level limit (SLA_V)	$SLA_V = 30dB$
		Front-back ratio (A_m)	$A_m = 30dB$
		Maximum directional gain ($G_{\max}$)	$G_{\max} = 8dBi$
System model	Carrier frequency (f_c)		$f_c = 30GHz$
	Bandwidth (W)		$W = 80MHz$
	Antenna configuration	BS	(4,8,2,1,1)/(4,8,2,2,2)
		UE	(2,2,2,1,1)
	Precoding	Analog	CRI-based beamforming
		Digital	Type I single/multi panel codebook
	Scheduler		Proportional fair scheduling per TTI
	Feedback		CSI sets with a periodicity of 5ms
	Receiver		Ideal interference estimation/MMSE-IRC
	Hybrid ARQ		Maximum of four transmissions
Simulation model	UE attachment		Based on RSRP
	Network layout		3D-UMa
	# of UEs per cell		20
	UE distribution	Indoor/outdoor distribution	Indoor: 80% Outdoor: 20%
		Horizontal distribution	Uniformly distributed
		Vertical distribution	$h_{UT} = 3(n_{fl} - 1) + 1.5$ where $n_{fl} \sim \mathcal{U}\{1, \mathcal{U}(4, 8)\}$
	UE speed		Indoor: 3km/h outdoor: 30km/h
	Traffic model		Full buffer

exclude the kth precoding matrix in BS ℓ, respectively. Note that the MMSE-IRC filter in (11) is given as

$$\mathbf{g}_{\ell,k} = \left(\tilde{\mathbf{H}}_{\ell,k}\right)^H \left(\frac{P}{|S_\ell|}\tilde{\mathbf{H}}_{\ell,k}\tilde{\mathbf{H}}_{\ell,k}^H + \sigma_n^2 \mathbf{I}_{N_r}\right)^{-1} \tag{12}$$

where $\tilde{\mathbf{H}}_{\ell,k} = \mathbf{H}_{\ell,k}\mathbf{W}_{\ell,k}^{(A)}\mathbf{W}_{\ell,k}^{(D)}$.

B. BASELINE PERFORMANCE EVALUATION FOR NR

This section evaluates the average spectral efficiency of 5G K-SimSys, as the antenna configurations are varied for massive MIMO. In particular, we first attempt to compare the baseline performance of two different types of CSI-RS transmission schemes with 'Type I single-panel' feedback. The results for multi-panels are covered in Section IV. Table 3 summarizes the simulation parameters for NR eMBB service in the urban macro-cell (UMa) environment [37]. A 3D channel model is essential for evaluating the performance of massive MIMO [21], [22], [36]. 5G K-SimSys provides its source code that has been calibrated for channel verification with the results in [21], [22], [36]. The 3D-SCM generates a long-term channel, one for each link, along with a short-term channel that varies with mobile speed. Furthermore, it considers the mmWave band at 30 GHz with the number of antennas $MNP = 64$ for each panel.

For $MNP = 64$, the average cellular spectral efficiency depends on the number of CSI-RS ports, i.e., N_1N_2P, for both CSI-RS transmission types. Recall that a specific pattern for antenna ports, i.e., N_1 and N_2, is specified in NR for the given number of antenna ports. Fig. 6 shows the average spectral efficiency for both types of CSI-RS transmissions on varying the number of CSI-RS ports. For $N_1N_2P = 64$, the performance is obtained by employing a fully digital beamforming structure in which all physical antenna elements are mapped into an individual port, i.e., one-to-one mapping between antenna element and port. However, the efficiency decreases with the smaller number of CSI-RS ports, as the degree of freedom that can be controlled by feedback is reduced. Because more feedback bits are employed for the nonprecoded CSI-RS transmission, its performance can be improved over the beamformed CSI-RS transmission as N_1N_2P increases. In contrast, the performance of the beamformed CSI-RS transmission can be improved by reducing N_1N_2P as digital beamforming becomes less effective within the sharper analog beam.

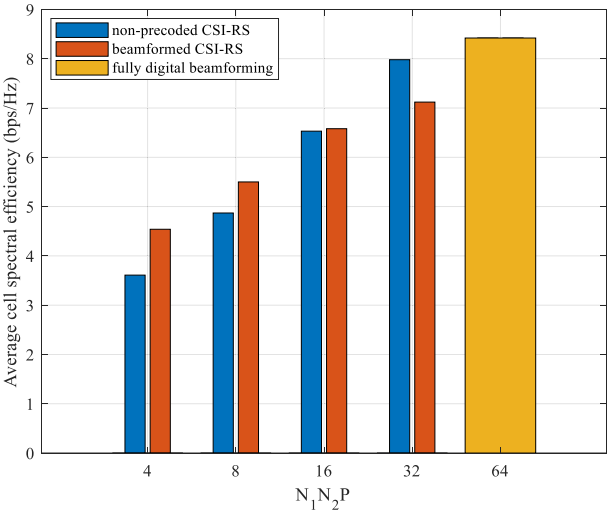

FIGURE 6. Average spectral efficiency as varying the number of CSI-RS ports [12].

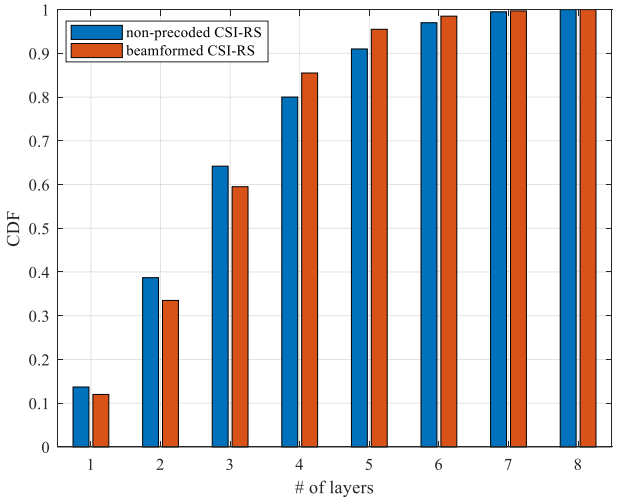

FIGURE 7. CDF for varying the number of layers: $N_1N_2P = 8$ [12].

Fig. 7 shows the distribution of the number of MU-MIMO layers (the number of users that has been selected for simultaneous transmissions assuming a single layer per UE) for $N_1N_2P = 8$. It is notable that the beamformed CSI-RS transmission allows for more layers, which results in selecting different users for each analog beam.

Fig. 8 illustrates the snapshot for beam maintenance while assuming that a specific UE is scheduled for certain slots. We observe that a reference UE is served by selecting a reception beam index 5, which has the highest RSRP starting from a slot number of 30. When the normalized RSRP 5 gradually decreases with time, two consecutive NACK messages are reported at slot numbers 42 and 45, respectively, eventually evoking beam maintenance. Then, P2 is applied to select beam index 3 at slot number 48. Subsequently, CSI feedback sets for the selected beam index 3 are determined. Fig. 8 also illustrates how the spectral efficiency of UE varies during beam maintenance. A seamless beam selection for beam maintenance is found to maintain spectral efficiency.

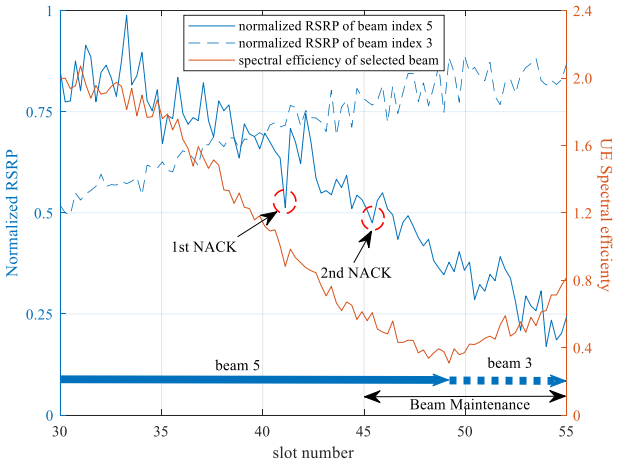

FIGURE 8. A snapshot for beam maintenance.

Next, we investigate the effect of vertical beamforming on inter-user interference (IUI) and inter-cell interference (ICI) in the FD-MIMO environment. Note that the line-of-sight zenith angle of departure (LoS-ZoD) depends on the height of base station, h_{BS}, in 3D-UMi and 3D-UMa scenarios. In the current model, LoS-ZoD is mainly centered around 90° in 3D-UMa environment. As h_{BS} increases, LoS-ZoD is shown to increase gradually, implying that most of the UEs fall under a limited angle span in the vertical dimension as compared to 3D-UMi. Therefore, it is necessary to make sharper vertical beams using more antenna elements to reduce IUI. Fig. 9 shows the average ICI-to-ICI plus IUI (ICI/(ICI+IUI)) as h_{BS} increases while fixing h_{UT}. As LoS-ZoD increases with h_{BS}, ICI is reduced. Furthermore, vertical sectorization with analog beamforming becomes less effective, i.e., its performance eventually converges to that of fully digital beamforming, as h_{BS} increases.

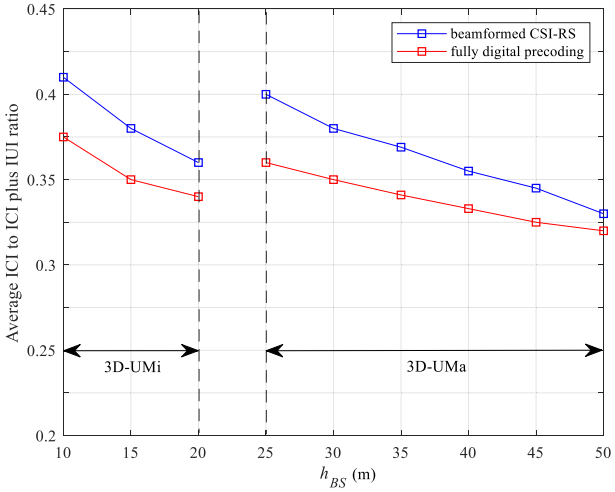

FIGURE 9. Average ICI/(ICI + IUI) ratio as varying the BS height in the different environments: $N_1N_2P = 8$.

IV. DEMONSTRATION FOR USE CASE: BAND-WISE ANALOG BEAMFORMING (BAB)

A. BAND-WISE ANALOG BEAMFORMING (BAB)

In this section, we introduce a notion of BAB, which countermeasures the mismatch effect of independent analog and digital beam selection for multi-user MIMO. Then, 5G K-SimSys is employed to implement a system-level simulator for evaluating a spectral efficiency gain achieved by BAB. Recognizing that a typical module in 5G K-SimSys could be reused to design the virtual modules for BAB, this section intends to present one particular useful case of exploiting the modular and flexible structure of 5G K-SimSys. The case will be used to demonstrate how powerful the underlying modular architecture is to structure the numerous new entities with individual objects of the same functionality layers.

As a wideband mmWave band suffers from frequency selectivity, its effect must be carefully taken into account in the course of implementing the hybrid beamforming structures [29]. Each UE is allocated with multiple bandwidth parts (BWPs), each of which is a group of contiguous physical resource blocks (PRBs). In the course of scheduling, however, only one BWP is activated, and its CSI feedback set is determined by each UE. Meanwhile, analog precoding is only applied to wideband; therefore, each BS must select the optimal wideband analog beamforming matrix, $\mathbf{W}^{(A)} = \left[\mathbf{W}^{(A)}_{(1)}, \mathbf{W}^{(A)}_{(2)}, \cdots, \mathbf{W}^{(A)}_{(N^{CSI}_{RES})}\right]^T$, which is then used as the set of the scheduled UEs. Furthermore, digital beamforming is determined only on the scheduled PRB, along with the wideband analog beam. Due to the limited number of analog beams that can be shared among all UEs in each TTI, e.g., $N^{CSI}_{RES} = 4$, some UEs might not be scheduled for their own reported beams, limiting the overall system performance.

Such a mismatch in beam allocation might result in further performance degradation due to the frequency selectivity in wideband analog beamforming. In other words, the current standards do not allow for joint analog and digital beam selection. In this section, we introduce the notion of BAB as a means to offset the effect of such a mismatch by exploiting both frequency and beam diversities simultaneously.

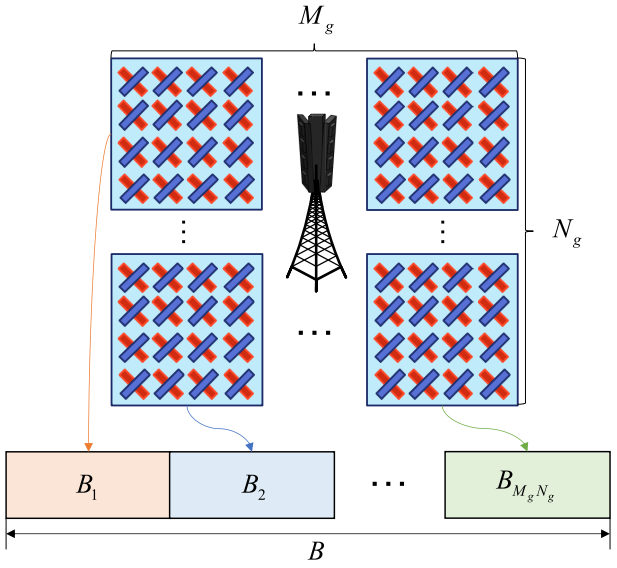

FIGURE 10. Multipanel-based bandwise analog beamforming (BAB): Illustration.

BAB divides a whole band into multiple narrow bands, each for independent analog beamforming. Then, different antenna ports are assigned to different subbands. For example, the overall bandwidth is equally divided into B subbands, while allocating N_{RES}^{CSI}/B antenna ports to each band. In NR specification, each BWP can be considered as a subband for BAB. As array gain is reduced with decreasing number of antenna elements per antenna port, analog beamforming becomes more sensitive towards inter-panel interference. However, multi-user diversity gain can be obtained if more beams are selected for the different subbands. Fig. 10 illustrates subband allocation for a multi-panel-based BAB, in which each panel supports different subband by dividing a whole band into M_gN_g subbands, one for each panel. Then, each UE reports the feedback set independently for each subband, which allows for frequency and beam diversity-aware flexible scheduling. The performance evaluation by 5G K-SimSys is shown in the following sections after discussing its implementation.

B. IMPLEMENTATION OF VIRTUAL MODULES FOR BAB

From an implementation viewpoint, the most important feature of 5G K-SimSys is reusability of the baseline modules centered around the main object **SIM**. For any new implementation scenario, some modules must be carefully redesigned and/or modified while reusing the existing functional blocks efficiently. Once UEs are connected, subbands are selected on a much longer period than the periodic reference signal. Selection of the individual analog beam for each subband implies that independent scheduler and hybrid ARQ processes can be employed for the different subbands. Therefore, each subband is subject to SINR calculation, requiring multiple parallel submodules to be redesigned. In fact, modules for Channel, Scheduling, and Performance can be redesigned or reused so that each module is performed independently on a band-wise basis. Due to the highly modular structure of functionalities for all objects, the existing simulator can be immediately modified by systematic module calls.

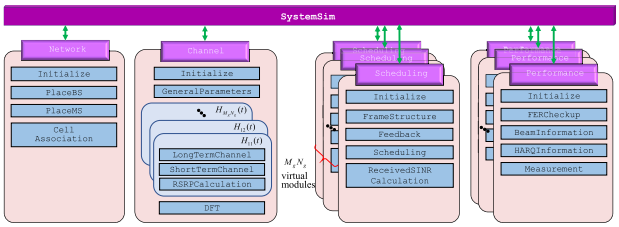

FIGURE 11. Virtual modules for BAB in 5G K-SimSys.

Fig. 11 shows the modular structure of the 5G K-SimSys for BAB, modified from that of the baseline simulator in Fig. 5. The same `Channel` submodule is reused for generating the channel matrices for all different panels. More specifically, let $\tilde{\mathbf{H}}_{mn}(t)$ denote a time-domain channel matrix for (m,n)th panel, $m = 1, 2, \cdots, M_g$; $n = 1, 2, \cdots, N_g$, which is given by a submatrix of the channel matrix for all antenna elements. Once a channel submatrix $\tilde{\mathbf{H}}_{11}(t)$ for a reference panel is generated by the baseline channel module, new submodules for all other channels $\{\tilde{\mathbf{H}}_{m,n}(t)\}_{m,n\neq 1}$ can be generated by considering the phase change due to the relative distance from the reference panel. Similarly, the same `Scheduling` and `Performance` modules are employed now for each subband. In other words, a simulator can be redesigned at the individual module and submodule levels while maintaining a baseline structure. As a feedback process is executed for each subband independently, the existing `Feedback` submodule can be also reused to create a virtual module for each panel. The overall performance is configured by `SystemSim` module, which collects the results from all virtual modules.

C. PERFORMANCE ANALYSIS

Assuming that $M_g = N_g = 2$, performance of BAB-based sharing is compared with that of the wideband analog beam (WAB)-based sharing that employs the 'Type I multi-panel' codebook. Referring to the band configuration in Fig. 10, a whole band is equally divided into four subbands for BAB. Fig. 12 shows the average cell spectral efficiency of both sharing schemes for the different number of UEs

per sector. When there are four UEs per sector, BAB achieves a performance gain of about 47% over WAB.

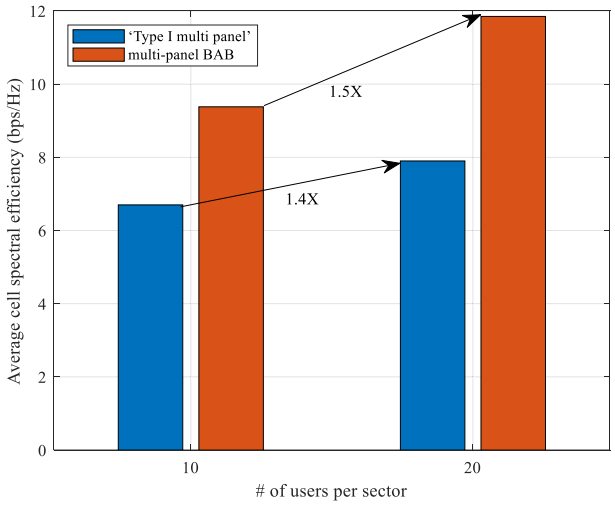

FIGURE 12. Average spectral efficiency as varying the number of users per sector: Wideband beam sharing vs. BAB-based beam sharing.

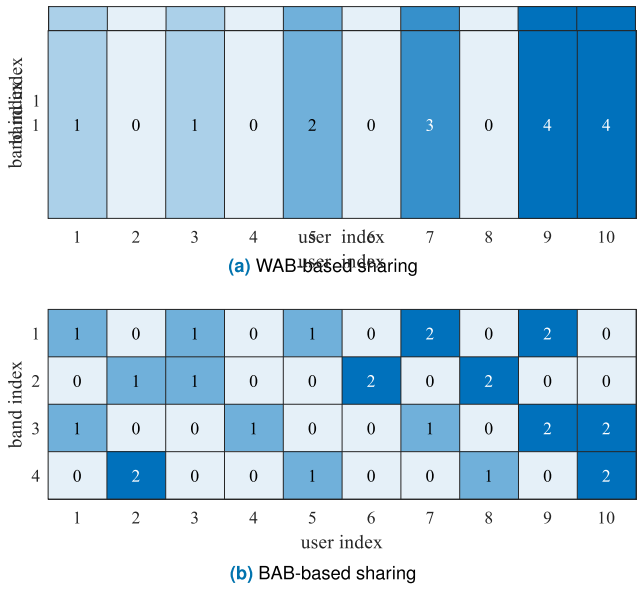

FIGURE 13. A snapshot for beam allocation.

Additional performance gain is observed with more numbers of UEs in each sector. This can be confirmed by investigating a snapshot of beam allocation for individual UEs for both schemes. In particular, Figs. 13(a) and (b) show specific snapshots for beam allocation with WAB and BAB-based sharing schemes, respectively. We assume that $N_{RES}^{CSI} = 4$ and 2 for WAB and BAB, respectively. Fig. 13(a) demonstrates the allocation of beams to individual UEs, where beam index 0 indicates no beam allocation. While generating rather sharper beams using all antenna elements with a single wideband, each beam tends to serve a limited number of UEs, i.e., one or two UEs. Furthermore, some UEs are not allocated to any beam, e.g., UEs 2, 4, 6, and 8, due to frequency selectivity. Meanwhile, two different UEs in the same beam can be supported by multi-user MIMO with digital beamforming. In contrast, Fig. 13(b) shows beam allocation for BAB with four subbands. We observe that different beams are selected in each subband. For example, UE 2 has two possible beams to use, beam 1 in subband 2 and beam 2 in subband 4. Thus, all UEs are served simultaneously over different subbands, indicating that both multi-user and multi-subband diversity can be achieved by BAB.

V. CONCLUSION

We discussed the implementation of 5G K-SimSys to evaluate the massive MIMO performance, including the related 3GPP New Radio specification details. Then, its actual performance has been demonstrated for the precoding matrices, e.g., 'Type I Single/Multi-Panel' codebook. As demonstrated in this study, system-level evaluation of massive MIMO is a good example to fully explore the detailed features in 5G K-SimSys. We evaluated the baseline performance of NR-MIMO using 5G K-SimSys. Furthermore, we compared the performance of the two types of CSI-RS transmissions by varying the number of antenna ports, and analyzed the effect of vertical beamforming on the interference according to the various FD-MIMO environments. In addition, the effect of vertical beamforming under the given UE distribution scenario was carefully evaluated for various system aspects of massive MIMO. In fact, it has been demonstrated that 5G K-SimSys is as a useful tool for a comprehensive system-level evaluation of massive MIMO, which involves the detailed system models in various environments.

Finally, we identified that implementing the same analog beam over the wideband limits the flexibility in scheduling. Therefore, we proposed a bandwise analog beamforming (BAB) scheme to improve a UE scheduling gain, allowing for both multi-user and multi-band diversity, despite the less antenna gain per panel. As demonstrated in this study, the BAB yields approximately 47% better performance than the NR with flexible scheduling. For its performance analysis, we showed how a typical module in 5G K-SimSys could be reused to design the virtual modules specialized for BAB. In fact, its modular and flexible structure turns out to be useful for introducing new features in the system level, without having to design and implement the whole processes from the scratch. As 5G K-SimSys is currently available for public use, it can serve as an open platform and testbed for evaluating the system-level performance of 5G systems.

REFERENCES

[1] J. C. Ikuno, M. Wrulich, and M. Rupp, "System level simulation of LTE networks," in *Proc. IEEE 71st Veh. Technol. Conf.*, Taipei, Taiwan, May 2010, pp. 1–5.

[2] L. Chen, W. Chen, B. Wang, X. Zhang, H. Chen, and D. Yang, "System-level simulation methodology and platform for mobile cellular systems," *IEEE Commun. Mag.*, vol. 49, no. 7, pp. 148–155, Jul. 2011.

[3] M. K. Müller, F. Ademaj, T. Dittrich, A. Fastenbauer, B. R. Elbal, A. Nabavi, L. Nagel, S. Schwarz, and M. Rupp, "Flexible multi-node simulation of cellular mobile communications: The Vienna 5G system level simulator," *EURASIP J. Wireless Commun. Netw.*, vol. 2018, no. 1, pp. 1–17, Dec. 2018.

[4] C. Mehlführer, J. Colom Ikuno, M. Šimko, S. Schwarz, M. Wrulich, and M. Rupp, "The Vienna LTE simulators—Enabling reproducibility in wireless communications research," *EURASIP J. Adv. Signal Process.*, vol. 2011, no. 1, pp. 1–14, Jul. 2011.

[5] M. Rupp, S. Schwarz, and M. Taranetz, *The Vienna LTE-Advanced Simulators: Up and Downlink, Link and System Level Simulation* (Signals and Communication Technology), 1st ed. Singapore: Springer, 2016.

[6] *Study on Channel Model for Frequencies From 0.5 to 100 GHz*, document 3GPP TR 38.901 V14.5.0, Rel-14, Jan. 2018.

[7] *Guidelines for Evaluation of Radio Interface Technologies for IMT-2020*, document Rep. ITU-R M.2412, Oct. 2017.

[8] M. Shafi, A. F. Molisch, P. J. Smith, T. Haustein, P. Zhu, P. De Silva, F. Tufvesson, A. Benjebbour, and G. Wunder, "5G: A tutorial overview of standards, trials, challenges, deployment, and practice," *IEEE J. Sel. Areas Commun.*, vol. 35, no. 6, pp. 1201–1221, Jun. 2017.

[9] S. Cho, S. Chae, M. Rim, and C. G. Kang, "System level simulation for 5G cellular communication systems," in *Proc. 9th Int. Conf. Ubiquitous Future Netw. (ICUFN)*, Milan, Italy, Jul. 2017, pp. 296–299.

[10] M. Han, J. W. Lee, C. G. Kang, and M. J. Rim, "5G K-SimSys: Open/modular/flexible system level simulator for 5G system," in *Proc. IEEE Int. Symp. Dyn. Spectr. Access Netw. (DySPAN)*, 2018, pp. 1–2, doi: 10.1109/DySPAN.2018.8610417.

[11] M. S. Han, J. W. Lee, C. G. Kang, and M. J. Rim, "System-level performance evaluation with 5G K-SimSys for 5G URLLC system," in *Proc. 16th IEEE Annu. Consum. Commun. Netw. Conf. (CCNC)*, 2019, pp. 1–5, doi: 10.1109/CCNC.2019.8651885.

[12] J. W. Lee, M. S. Han, C. G. Kang, and M. J. Rim, "5G K-SimSys for system-level evaluation of massive MIMO," in *Proc. 16th IEEE Annu. Consum. Commun. Netw. Conf. (CCNC)*, 2019, pp. 1–6, doi: 10.1109/CCNC.2019.8651802.

[13] M. Mezzavilla, M. Zhang, M. Polese, R. Ford, S. Dutta, S. Rangan, and M. Zorzi, "End-to-end simulation of 5G mmWave networks," *IEEE Commun. Surveys Tuts.*, vol. 20, no. 3, pp. 2237–2263, 3rd Quart., 2018.

[14] T. L. Marzetta, "Noncooperative cellular wireless with unlimited numbers of base station antennas," *IEEE Trans. Wireless Commun.*, vol. 9, no. 11, pp. 3590–3600, Nov. 2010.

[15] F. Rusek, D. Persson, B. Kiong Lau, E. G. Larsson, T. L. Marzetta, and F. Tufvesson, "Scaling up MIMO: Opportunities and challenges with very large arrays," *IEEE Signal Process. Mag.*, vol. 30, no. 1, pp. 40–60, Jan. 2013.

[16] E. G. Larsson, O. Edfors, F. Tufvesson, and T. L. Marzetta, "Massive MIMO for next generation wireless systems," *IEEE Commun. Mag.*, vol. 52, no. 2, pp. 186–195, Feb. 2014.

[17] L. Lu, G. Y. Li, A. L. Swindlehurst, A. Ashikhmin, and R. Zhang, "An overview of massive MIMO: Benefits and challenges," *IEEE J. Sel. Topics Signal Process.*, vol. 8, no. 5, pp. 742–758, Oct. 2014.

[18] Y. Kim, H. Ji, J. Lee, Y.-H. Nam, B. L. Ng, I. Tzanidis, Y. Li, and J. Zhang, "Full dimension MIMO (FD-MIMO): The next evolution of MIMO in LTE systems," *IEEE Wireless Commun.*, vol. 21, no. 2, pp. 26–33, Apr. 2014.

[19] Y.-H. Nam, B. Ng, K. Sayana, Y. Li, J. Zhang, Y. Kim, and J. Lee, "Full-dimension MIMO (FD-MIMO) for next generation cellular technology," *IEEE Commun. Mag.*, vol. 51, no. 6, pp. 172–179, Jun. 2013.

[20] H. Ji, Y. Kim, J. Lee, E. Onggosanusi, Y. Nam, J. Zhang, B. Lee, and B. Shim, "Overview of full-dimension MIMO in LTE-advanced pro," *IEEE Commun. Mag.*, vol. 55, no. 2, pp. 176–184, Feb. 2017.

[21] B. Mondal, T. Thomas, E. Visotsky, F. Vook, A. Ghosh, Y.-H. Nam, Y. Li, J. Zhang, M. Zhang, Q. Luo, Y. Kakishima, and K. Kitao, "3D channel model in 3GPP," *IEEE Commun. Mag.*, vol. 53, no. 3, pp. 16–23, Mar. 2015.

[22] *Study on Elevation Beamforming/Full-Dimension (FD) Multiple Input Multiple Output (MIMO) for LTE*, document 3GPP TR 36.897 V13.0.0, Rel-13, Jun. 2015.

[23] A. F. Molisch, V. V. Ratnam, S. Han, Z. Li, S. L. H. Nguyen, L. Li, and K. Haneda, "Hybrid beamforming for massive MIMO: A survey," *IEEE Commun. Mag.*, vol. 55, no. 9, pp. 134–141, Sep. 2017.

[24] A. Goldsmith, *Wireless Communications*. Cambridge, U.K.: Cambridge Univ. Press, Aug. 2005.

[25] D. Tse and P. Viswanath, *Fundamentals of Wireless Communication*. Cambridge, U.K.: Cambridge Univ. Press, May 2005.

[26] S. Han, C.-L. I, Z. Xu, and C. Rowell, "Large-scale antenna systems with hybrid analog and digital beamforming for millimeter wave 5G," *IEEE Commun. Mag.*, vol. 53, no. 1, pp. 186–194, Jan. 2015.

[27] S. Park, A. Alkhateeb, and R. W. Heath, Jr., "Dynamic subarrays for hybrid precoding in wideband mmWave MIMO systems," *IEEE Trans. Wireless Commun.*, vol. 16, no. 5, pp. 2907–2920, May 2017.

[28] O. E. Ayach, S. Rajagopal, S. Abu-Surra, Z. Pi, and R. W. Heath, Jr., "Spatially sparse precoding in millimeter wave MIMO systems," *IEEE Trans. Wireless Commun.*, vol. 13, no. 3, pp. 1499–1513, Mar. 2014.

[29] A. Alkhateeb, J. Mo, N. Gonzalez-Prelcic, and R. W. Heath, Jr., "MIMO precoding and combining solutions for millimeter-wave systems," *IEEE Commun. Mag.*, vol. 52, no. 12, pp. 122–131, Dec. 2014.

[30] F. Sohrabi and W. Yu, "Hybrid digital and analog beamforming design for large-scale antenna arrays," *IEEE J. Sel. Topics Signal Process.*, vol. 10, no. 3, pp. 501–513, Apr. 2016.

[31] A. Zaidi, F. Athley, J. Medbo, U. Gustavsson, G. Durisi, and X. Chen, *5G Physical Layer: Principles, Models and Technology Components*. New York, NY, USA: Academic, 2018.

[32] *Physical Layer Procedures for Data*, document 3GPP TS 38.214 V15.3.0, Rel-15, Oct. 2018.

[33] Y. Huang, Y. Li, H. Ren, J. Lu, and W. Zhang, "Multi-panel MIMO in 5G," *IEEE Commun. Mag.*, vol. 56, no. 3, pp. 56–61, Mar. 2018.

[34] Y. Choi, J. Lee, M. Rim, C. G. Kang, J. Nam, and Y.-J. Ko, "System-level performance of limited feedback schemes for massive MIMO," *ETRI J.*, vol. 38, no. 2, pp. 280–290, Apr. 2016.

[35] Y.-N.-R. Li, B. Gao, X. Zhang, and K. Huang, "Beam management in millimeter-wave communications for 5G and beyond," *IEEE Access*, vol. 8, pp. 13282–13293, 2020.

[36] *Study on 3D Channel Model for LTE*, document 3GPP TR 36.873 V12.0.0, Rel-12, Sep. 2014.

[37] *Study on New Radio Access Technology Physical Layer Aspects*, document 3GPP TR 38.802 V14.2.0, Rel-14, Sep. 2017.

JAEWON LEE received the B.S. degree from the School of Information and Communication Engineering, Chungbuk National University, in 2014. He is currently pursuing the unified M.S. and Ph.D. degrees with the Department of Telecommunication System Technology, Korea University (KU). His research interests include massive MIMO and waveforms.

MINSIG HAN received the B.S. degree in electrical engineering from Korea University (KU), in 2016, where he is currently pursuing the unified M.S. and Ph.D. degrees in electrical engineering. He is honored with the 2017 Global Ph.D. Fellowship (GPF) and funded by the National Research Foundation (NRF) for his research. His research interests include (machine learning-based) cross-layer design and optimization for 5G/6G wireless communication systems.

MINJOONG RIM received the B.S. degree in electronics engineering from Seoul National University, Seoul, South Korea, in 1987, and the Ph.D. degree in electrical and computer engineering from the University of Wisconsin–Madison, USA, in 1993.

From 1993 to 2000, he worked with Samsung Electronics. He is currently a Professor with Dongguk University, Seoul. His research interests include mobile and wireless communications.

CHUNG G. KANG (Senior Member, IEEE) received the B.S. degree in electrical engineering from the University of California, San Diego, in 1987, and the M.S. and Ph.D. degrees in electrical and computer engineering from the University of California, Irvine, in 1989 and 1993, respectively. Since March 1994, he has been with the Department of Radio Communication and Engineering, and later with the Department of Electrical Engineering, Korea University, Seoul, Republic of Korea, where he is currently a Full Professor. He has over 200 refereed publications in international journals and conference proceedings in the fields of mobile communication and wireless networks, while holding over 100 patents. He also coauthored a reference textbook on the MIMO-OFDM wireless system, entitled *MIMO-OFDM Wireless Communication with MATLAB* (Wiley, 2010). His research interests include next generation mobile radio communication systems and broadband wireless networks with an emphasis on cross-layer design and optimization. His recent research has been focused on massive MIMO, grant-free non-orthogonal multiple access, dynamic spectrum access, mobile caching networks, and AI-based communication system design. He is a Senior Member of IT and VT, a KICS Fellow, and a member of the National Academy of Engineering of Korea. He has served as the Chair for the KICS Mobile Communication Technical Activity Group, the President for KICS, and the Chair for the Wireless Technology Committee in 5G Forum of Korea. He served as the Chair for the 2.3GHz IMT-WiBro Project Group (PG702), Telecommunications Technology Association (TTA), which is a Standard Development Organization (SDO), South Korea. As a recipient of the Dr. Irwin Jacobs Award sponsored by Qualcomm Inc. for his contribution to researches on mobile communication technologies.